PAPER

Impact of the zinc complexation of polytopic polyaza ligands on the interaction with double and single stranded DNA/RNA and antimicrobial activity†

Jorge González-García, Dr., [ID] *[a] Carolina Galiana, Dr.,[b]
M. Auxiliadora Dea-Ayuela, Prof.,[b] Marijana Radić Stojković, Dr.,[c]
Sonia López-Molina, Dr., [ID] [a] Cristina Galiana-Roselló, Dr.,[a] Salvador Blasco, Dr.,[a]
Ivo Piantanida, Dr. [ID] *[c] and Enrique García-España, Prof. [ID] *[a]

Metal complexes have gained a huge interest in the biomedical research in the last decade because of the access to unexplored chemical space with regards to organic molecules and to present additional functionalities to act simultaneously as diagnostic and therapeutic agents. Herein, we evaluated the interaction of two polytopic polyaza ligands and their zinc complexes with DNA and RNA by UV thermal denaturation, fluorescence and circular dichroism spectroscopic assays. The zinc coordination was investigated by X-ray diffraction and afforded the structure of the binuclear zinc complex of **PYPOD**. Thermal denaturation of DNA and RNA and fluorimetry analysis revealed preferential binding of the zinc-**PHENPOD** complexes towards GC-containing DNA in contrast to the free ligands. On the other hand, **PYPOD** metal complexes, compared to the free ligand, stabilized AT-based DNA (B-form) better than AU-RNA (A-form). With regards to single stranded RNA, the binuclear complex of **PHENPOD** and the free ligand can efficiently identify polyadenylic acid (poly A) among other RNA sequences by circular dichroism spectroscopy. The antimicrobial activity in *S. aureus* and *E. coli* bacteria showed the highest activity for the free ligands and their trinuclear zinc complexes. This work can provide valuable insights into the impact of the nuclearity of polytopic polyaza ligands in the binding to DNA/RNA and the antimicrobial effect.

Introduction

During the past decades, metal complexes have become essential drugs in a broad range of therapies, covering cancer, pathogenic infections, diabetes, anti-inflammatory, and neurological disorders.[1–3] Despite the clinical success of metal complexes for cancer, the landscape of inorganic compounds has been largely ignored for antimicrobial applications.[4] Only, bismuth and silver-based complexes are currently used for treating microbial infections for *Helicobacter pylori* and topical wounds respectively.[5–7] Nevertheless, the appearance of multi-drug resistant microbes summed to the lack of drug candidates in clinical trials as antibiotics have prompted the scientific community to investigate non-organic compounds such as metal complexes. Recent studies have highlighted the ability of metal complexes to access underexplored chemical space for drug development[8,9] and act through novel mechanisms of action.[10] Subsequent antimicrobial drug screening campaigns indicated a higher hit-rate of metal complexes towards pathogens in comparison to natural and organic molecules.[11,12]

The vast majority of the metal complexes for therapeutical applications are mononuclear species, while polynuclear ones are poorly explored. In many cases, multinuclear complexes improved the biological activity of their mononuclear counterparts. For instance, the trinuclear platinum complex **BBR3464** can overcome Cisplatin resistance in several cancer cell lines.[13] Moreover, polynuclear complexes can show a synergetic and/or complementary effect between the metals when binding to biomolecules such as DNA, RNA, lipids or proteins as well as present additional functionalities such as imaging.[14]

Our team and other groups have extensively investigated polynuclear complexes, with particular attention to first-row

[a]*Institute of Molecular Science, University of Valencia, Department of Inorganic Chemistry, 46009 Paterna, Spain. E-mail: jorge.gonzalez@uv.es*

[b]*Department of Pharmacy, CEU Cardenal Herrera University, Ramón y Cajal s/n, 46115 Alfara del Patriarca, Spain*

[c]*Division of Organic Chemistry & Biochemistry, Ruđer Bošković Institute, P. O. Box 180, 10002 Zagreb, Croatia*

metals such as zinc, copper and manganese.[15–21] Recently, we described how the formation of binuclear complexes modulated the interaction of several ligands with DNA/RNA.[22] We explored the increase of the antioxidant activity of polyaza binuclear manganese complexes in comparison with the mononuclear counterparts.[23]

In addition, we developed two polytopic polyaza ligands (**PYPOD** and **PHENPOD**, Scheme 1) and explored the zinc,[24] copper,[25,26] and manganese[23] coordination in addition to the interaction with duplex (ds) DNA/RNA.[27,28] Herein, we report the interaction of these ligands (see Scheme 1) and their mono- and polynuclear zinc metal complexes with the double and single stranded DNA/RNA by UV thermal, fluorescence emission and circular dichroism spectroscopies. The ligands form mono-, bi- and trinuclear complexes in solution according to potentiometry, photophysical and NMR studies. Moreover, we have characterised the structure of the binuclear zinc complex of **PYPOD** by X-ray analysis. Finally, the antibacterial activity of all the systems has been assessed in Gram-positive and Gram-negative bacteria.

Results and discussion

Synthesis and zinc coordination

The synthesis and characterisation of both ligands as well as their zinc coordination were reported in ref. 24. In brief, **PYPOD** and **PHENPOD** form mono-, bi- and trinuclear zinc complexes depending on the [M] : [L] molar ratio, the pH and the total concentration of the metal and ligand. We observed the formation of mono- and binuclear species above pH 3 for both ligands using 1 : 1 and 2 : 1 molar ratio. When using a 3 : 1 molar ratio, the trinuclear species are formed above pH 6.0 for **PHENPOD** and pH 9.0 for **PYPOD**. Using the stability constants, the speciation was calculated for the different molar ratio M : L used and at pH 7.4. For M : L 1 : 1, **PYPOD** has ZnH_2L and Zn_2HL as major species while **PHENPOD** shows ZnH_2L and Zn_2L. The species Zn_2L was formed almost quantitatively for both ligands at pH 7.4 in ratio M : L 2 : 1. For the highest molar ratio M : L 3 : 1, **PYPOD** presents only the Zn_2L species while **PHENPOD** presents the Zn_2L species and a minor contribution of the dihydroxylated trinuclear $Zn_3L(OH)_2$ species. A detailed explanation of the speciation, stability constants and zinc coordination are reported in ref. 24.
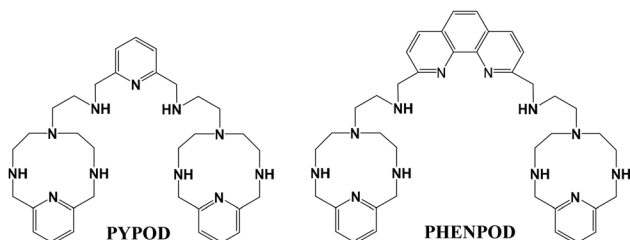
Solid state analysis

We obtained suitable crystals for X-ray analysis of the binuclear Zn^{2+} complex with **PYPOD** from the slow evaporation in H_2O–EtOH solution. In the crystal structure, the ligand **PYPOD** is forming the complex with formula $[Zn_2\mathbf{PYPOD}Cl]^{3+}$ (Table S1 in ESI†) in which each zinc atom is coordinated to one of the macrocyclic cavities. The complex is asymmetric as envisaged by the uneven number (11) of nitrogen donor atoms present in the ligand structure. Zn(1) is coordinated in an octahedral fashion to five nitrogen atoms, and to a chlorine atom, Cl(5) (see Fig. 1). On the other hand, Zn(2) is octahedrally coordinated by six nitrogen atoms, with the involvement of the nitrogen atom of the central pyridine spacer N(6) (Fig. 1). This coordination site exhibits a geometry very close to related mononuclear complexes of ligands containing just one macrocyclic unit and a 2-substituted pyridine linked to the aminoethyl pendant arm through a methylene bridge previously reported by us.[29] The coordination to the two zinc atoms imposes a tight geometry to the whole complex, in which **PYPOD** adopts a twisted conformation. Both zinc atoms present bond lengths and angles very similar to each other, Zn–N bond distances range from 2.06 to 2.28 Å (see Table S2 in ESI†). In both cases, the shortest bonds are those involving the pyridine nitrogen. Interestingly, Cl(5) is connected to a sodium atom which connects together two $[Zn_2\mathbf{PYPOD}Cl]^{3+}$ units and one perchlorate moiety which forms the "supercomplex"[30–32] $\{[Zn_2\mathbf{PYPOD}Cl]_2Na(ClO_4)\}^{6+}$ (see Fig. 2). The asymmetric unit is composed of half of the "supercomplex" along with three perchlorate anions and one water molecule.

DNA/RNA binding studies of Zn^{2+} complexes of PYPOD and PHENPOD

UV thermal denaturation experiments. First, we studied the interaction of the mono-, bi- and trinuclear Zn^{2+} complexes of the polytopic ligands with double-stranded DNA and RNA by UV thermal denaturation. These helical models contain different base composition that result in distinctive groove dimensions. The binding study was carried out with calf

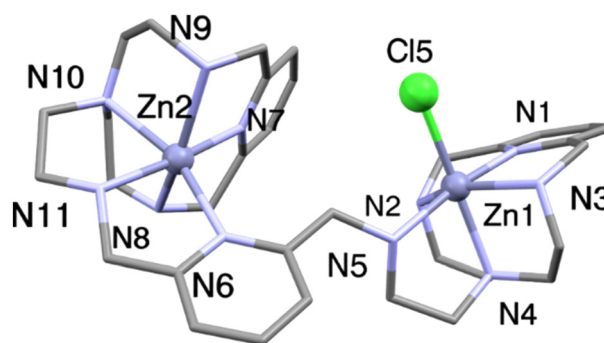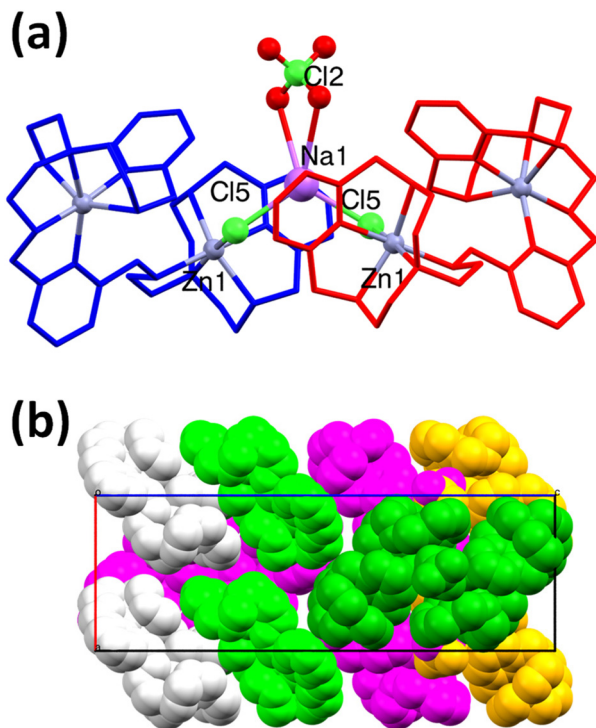
Scheme 1 Studied ligands.

Fig. 1 Mixed capped sticks/ball representation of the of the structure $[Zn_2\mathbf{PYPOD}Cl]_2\cdot Na\cdot 7(ClO_4)\cdot 2(H_2O)$. Hydrogen atoms, perchlorate, water and sodium moieties omitted for clarity.
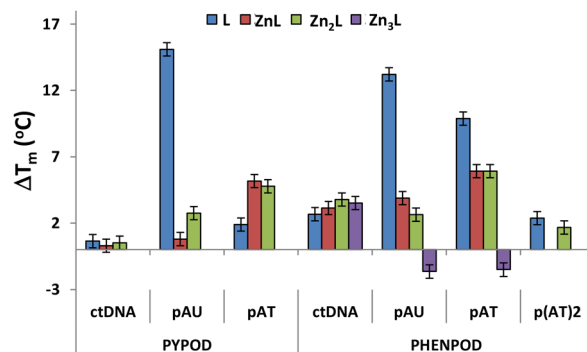
Fig. 2 (a) Mixed capped sticks/ball representation of the "supercomplex" $\{[Zn_2\mathbf{PYPOD}Cl]_2Na(ClO_4)\}^{6+}$ of the structure $[Zn_2\mathbf{PYPOD}Cl]_2\cdot Na\cdot 7$ $(ClO_4)\cdot 2(H_2O)$. Hydrogen atoms, counter ions and water molecules omitted for clarity. (b) Packing of "supercomplex", coloured by symmetry operation. Hydrogen atoms, anions and water molecules are omitted for clarity.

Fig. 3 ΔT_m values of **PYPOD**, **PHENPOD** and the corresponding zinc complexes with ds-polynucleotides.

thymus DNA (ctDNA), the homopolymer poly dA–poly dT, the alternating polymer poly d(AT)$_2$, as models for B-DNA, and poly rA–poly rU (RNA), as a model for A-form of nucleic acid.[33] The potentiometric analysis allowed us to identify the species in solution at the pH value[21] in which the assays were conducted, with the mononuclear species being predominant at a 1 : 1 molar ratio (L : M), the binuclear ones at a 1 : 2 molar ratio (L : M) and even the trinuclear species formed when using a 1 : 3 molar ratio for **PHENPOD**. The thermal denaturation experiments were conducted at two different molar ratios of L : ds-polynucleotide, 1 : 10 and 1 : 5 but only the former have been shown because both ratios provide similar results.

In general, both ligands induced a higher stabilisation effect as free ligands except for the interaction of **PYPOD** with poly dA–poly dT and **PHENPOD** with ctDNA (Fig. 3). The higher stabilisation effect induced by the ligands in contrast with the metal complexes suggests that the driving force of the interaction is mainly due to hydrogen bonding and/or electrostatics. The highly charged ligands interact strongly with the phosphate backbone and nucleobases (+4.19 and +4.33 for **PYPOD** and **PHENPOD** respectively at pH 7) whilst the metal coordination partially hinders the protonated amine groups and exerts a lower electrostatic interaction.

Intriguingly, the higher stabilisation of the zinc complex of **PYPOD** with AT-based polynucleotide indicates a different and

specific binding interaction with this nucleic acid with regards to ctDNA or AU-RNA. Considering the features of poly dA–poly dT with a narrower and deeper minor groove compared to a common B-form, it could be suggested that the coordination with the zinc ions allows for a better accommodation of the metal complexes within the minor groove and more efficient hydrophobic and van der Waals interactions.

Surprisingly, the trinuclear zinc complexes of **PHENPOD** modulate the interaction towards the destabilization of both AT- and AU-based polynucleotides (Fig. 3 purple bar), suggesting that the third Zn^{2+} possesses an unsaturated coordination sphere and interacts with A-only-based duplex probably *via* coordinative binding. However, thermal denaturation analysis revealed that zinc complexes of **PHENPOD** stabilised better ctDNA than the free ligand. It is probably the result of the mixed base-pair composition of that natural polynucleotide (42% GC base pairs and 58% AT base pairs). In addition, we performed thermal denaturation experiments with the metal salts to exclude their potential influence on DNA/RNA stabilisation. The analysis showed slight or negligible stabilisation of polynucleotides even at the highest molar ratios compared to those used with the metal complexes.

Fluorescence assays of compounds with DNA/RNA. We then utilised fluorimetric titrations to estimate the strength of the
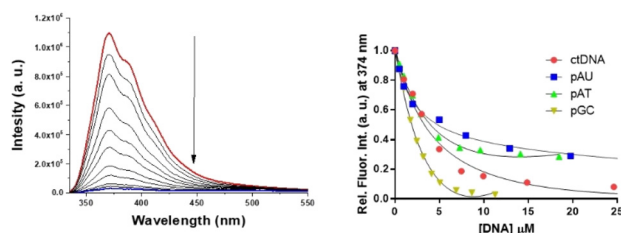
Fig. 4 Fluorimetric titration of Zn$_3$**PHENPOD** with poly dG–poly dC, c = 1×10^{-5} M, λ_{exc} = 320 in sodium cacodylate buffer I = 0.05 M, pH = 7.0. Red spectrum corresponds to the initial titration and blue spectrum to last one (left panel). Fitting of the titrations of Zn$_3$**PHENPOD** with all ds-polynucleotides (right panel).

interaction of the zinc-**PHENPOD** complexes with double- (ds-) and single-stranded (ss-) DNA/RNA. The addition of ds- and ss-polynucleotides to solution containing the mono-, the bi- or the trinuclear zinc complex of **PHENPOD** yielded the quenching of their fluorescence (see Fig. 4 and S1–8 in ESI†). The binding affinity values obtained from fluorescence experi-

Table 1 Values of the binding constants (log K_a) of zinc-**PHENPOD** complexes of with ds- and ss-polynucleotides calculated from the fluorimetric titrations (λ_{exc} = 320 nm, λ_{em} = 374 nm, c = 1 × 10^{-5} M) at pH 7.4 (sodium cacodylate buffer, I = 0.05 M)

	ZnPHENPOD	**Zn$_2$PHENPOD**	**Zn$_3$PHENPOD**
ctDNA	4.63[a]	4.67	4.73
Poly rA–poly rU	4.47	4.87	4.99
Poly dA–poly dT	—	4.75	4.74
Poly dG–poly dC	5.43	5.56	4.88
Poly A	5.06	5.13	5.33
Poly G	4.76	4.67	5.27
Poly C	2.99	3.71	3.58
Poly U	N.C.[b]	5.22	6.25

[a] Value error log K ± 0.5. [b] The value was not determined.

ments are shown in Table 1 and are, in general, higher for poly dG–poly dC compared to other DNAs and RNAs. This result is consistent with the better stabilising effect of ctDNA (42% GC base pairs) shown by the metal complexes compared to the free **PHENPOD** (Fig. 3).

In addition, the values obtained ranged within the same order of the free ligand obtained at slightly lower pH (see ref. 24) indicating that the coordination do not enhance the binding affinity towards duplexes.
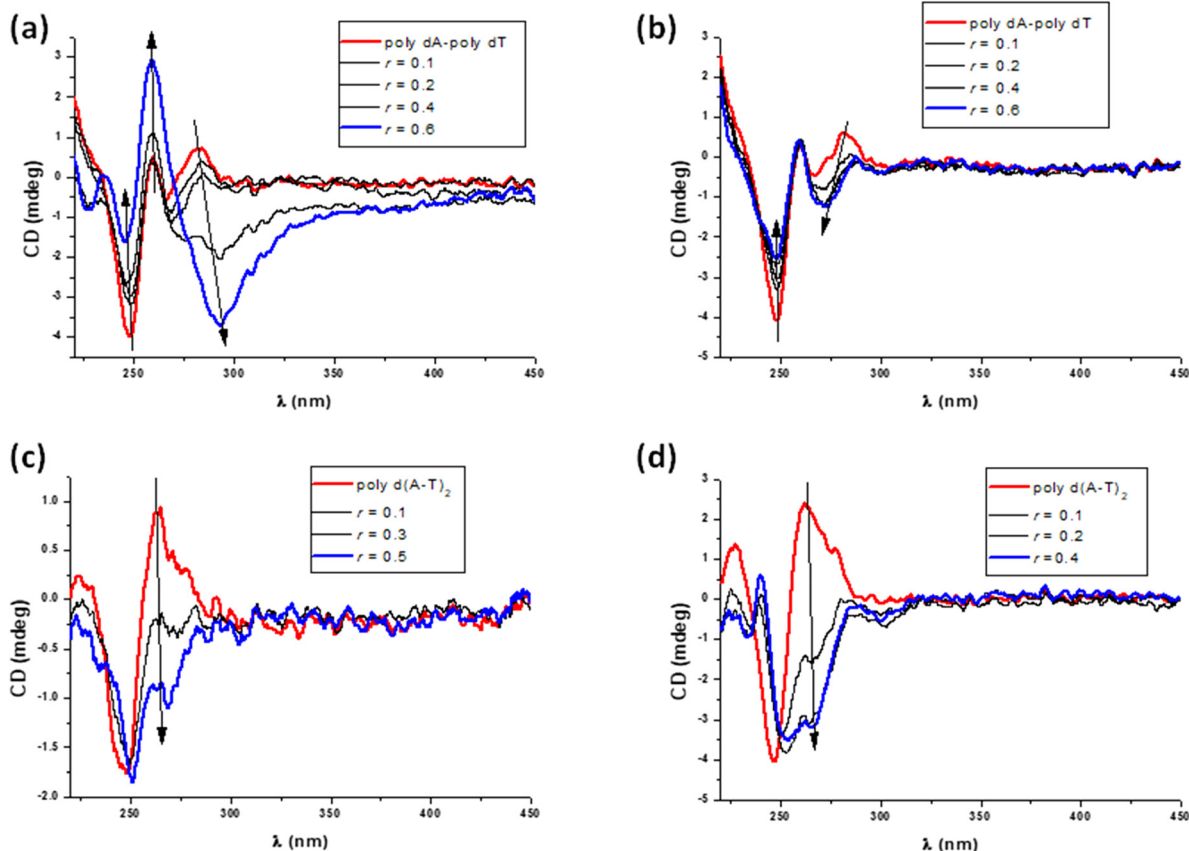
We also explored the interaction with single-stranded RNA polymers (poly A, poly G, poly C and poly U). All of them, except poly U, form well-organised helical structures in solution (Na Cacodylate, I = 0.05 M, pH = 7.4) due to the stacking between bases.

Addition of all ss-polymers induced a decrease in the fluorescence emission as it occurred with ds-polynucleotides (Fig. 4 and S5–8†) and the binding affinities were determined and collected in Table 1. The values of binding affinity of mono-, bi- and trinuclear complexes are comparable for poly A and poly G. However, those become higher upon increasing the nuclearity for poly C and poly U suggesting that the metal confers additional interactions towards these specific ss-polynucleotides. Zn$_3$**PHENPOD** displayed the highest affinity

Fig. 5 CD titration of poly dA–poly dT with (a) **PHENPOD** and (b) Zn$_2$**PHENPOD** or poly d(A−T)$_2$ with (c) **PHENPOD** and (d) Zn$_2$**PHENPOD** at different molar ratios r = [compound]/[polynucleotide] ([polynucleotide] = 1.0 × 10^{-5} M, buffer sodium cacodylate, I = 0.05 M at pH 7.4, compound is **PHENPOD** or Zn$_2$**PHENPOD**.

towards poly U (at least one order of magnitude) compared to other single-stranded RNAs.

Circular dichroism studies of the compounds with DNA/RNA. In order to get insight into the conformational changes of the secondary structure of polynucleotides, circular dichroism studies were performed with the most representative binuclear species of **PHENPOD** (Zn₂**PHENPOD**) and the ligand alone (**PHENPOD**). Additionally, the appearance of induced CD signals (ICD) provides information about the binding mode between the ligands and the binuclear zinc complexes to polynucleotides.

Addition of either **PHENPOD** or Zn₂**PHENPOD** to a solution of ctDNA showed similar changes in the CD spectra, namely, a decrease in the CD band intensity at 275 nm and a bathochromic shift of this positive band with an increase of the ratio, *r* (Fig. S9†).

Intriguingly, experiments performed with AT-based polynucleotides showed different behaviour upon addition of the ligand or the zinc complex (Fig. 5). In the titration of poly dA–poly dT with **PHENPOD** at a higher ratio, *r* (*r* > 0.2, Fig. 5), a negative ICD band centred around 300 nm appeared in addition to an increase of the CD band at 260 nm. Similar changes indicative of mild polynucleotide condensation were visible in the titration of the same polynucleotide with **PYPOD** (see ref. 25).

The zinc complex Zn₂**PHENPOD** showed minor changes in the polynucleotide CD maxima at 260 and 280 nm (see Fig. 5), suggesting that the conformation adopted by the metal complex hampers the interaction with this polynucleotide. In contrast to AT homopolymer, addition of either the ligand or the metal complex to solutions of alternating poly d(A–T)₂ caused an inversion of the CD polynucleotide band at 260 nm. This could be the result of either a significant impact on DNA conformation or a strongly negative ICD spectrum of **PHENPOD** in that range (see Fig. 5).

Both GC-based polynucleotides showed minor and similar variations in the CD spectra (a small decrease (see Fig. S12†) or increase (Fig. S13†) in intensity of the CD band at 260 nm) upon addition of **PHENPOD** or Zn₂**PHENPOD**. It is worth mentioning that poly A–poly U did not experience any variation of the CD spectra upon addition of either the ligand or the metal complex (Fig. S10†).

To obtain further information about the binding mode of the metal complexes towards single-stranded polynucleotides, we performed CD experiments with **PHENPOD** and its binuclear complex. CD titrations with poly C, poly G and poly U exhibited a decrease in the CD band intensity at 260 nm suggesting minor changes in their conformation (Fig. S14–S16†). Contrarily, both ligand and metal complex induced almost the complete loss of conformation of poly A (see a collapse in CD band intensities at 260 and 245 nm in Fig. S17†). This could result from different binding interactions (potential for hydrogen bonds, van der Waals forces) compared to the other used ss-polynucleotides.

Bacterial activity. To assess the antibacterial capacity of the ligands and the metal complexes, we evaluated bacterial viability by monitoring the bacterial growth through the optical density at 600 nm. We selected two bacteria strains of different origins, the Gram-positive *S. aureus* and the Gram-negative *E. coli*.

We observed a concentration dependent activity for all the systems in *E. coli* (Fig. 6). As shown in Fig. 6, the most active systems were the free ligands and the zinc complexes of both ligands at the highest concentration used (100 μM). At a fixed treatment concentration of 25 μM, **PHENPOD** shows the highest inhibitory effect with 17% of cell viability followed by its mononuclear zinc complex (29%), binuclear complex (33%) and trinuclear complex (37%). The same trend was observed for **PYPOD** and their corresponding zinc complexes, suggesting that the increase of the zinc nuclearity in these polyaza complexes reduces the inhibitory effect in *E. coli*. However, **PHENPOD** and its trinuclear zinc complex showed a higher inhibitory effect at 50 μM than the mono- and binuclear complex of **PHENPOD** (Fig. 6b).

In contrast to *E. coli*, assays with *S. aureus* showed cell inhibition of all, free ligands and their mono-, bi- and trinuclear zinc complexes, only at 100 μM (see Fig. S18 and S19†), suggesting that this bacteria strain is less sensitive than *E. coli*. Considering the type of bacteria, polyamine-based ligands and the zinc complexes exhibit a higher antibacterial effect on Gram-negative bacteria, although the bacteria present the outer membrane of glycerophospholipids, which hinders the uptake and effect of the antibiotics.
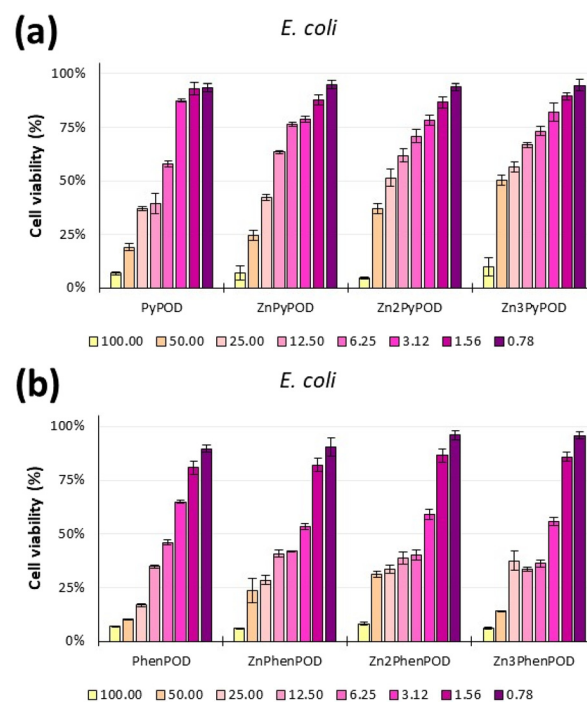
Fig. 6 Cell viability analysis in *E. coli* based on the optical density at 600 nm for **PYPOD**, Zn**PYPOD**, Zn₂**PYPOD** and Zn₃**PYPOD** (top panel) and for **PHENPOD**, Zn**PHENPOD**, Zn₂**PHENPOD** and Zn₃**PHENPOD**. Legends represent the concentration in μM.

Conclusions

Metal complexes have gained a huge interest in the biomedical research in the last decade because they provide access to chemical space unexplored by organic molecules. Here we have studied the interaction of mono- and polynuclear zinc complexes of two polytopic polyaza ligands (**PYPOD** and **PHENPOD**) with double and single stranded DNA/RNA and evaluated their antibacterial inhibitory effect.

The crystal structure of the binuclear zinc complex of **PYPOD** ([Zn₂**PYPOD**Cl]³⁺) shows asymmetric coordination sites, in agreement with the analysis of the stability constants obtained in previous works.[21] Both zinc centres are coordinated to the four nitrogen atoms of each macrocyclic moiety and the nitrogen of the pendant arm, while one zinc is coordinated to the central pyridine spacers and the other one to a chloride.

In general, the free ligands show a higher stabilisation effect on DNA and RNA duplexes than the mono-, bi- and trinuclear zinc complexes. It indicates that the interaction is governed by the net charge of the systems since the ligands possess a higher net charge than the metal complexes at the pH of study. Only the polynuclear zinc complexes of **PYPOD** exhibit a stronger stabilisation for poly dA–poly dT, which can be rationalised because the zinc complexes are better accommodated into the narrower and deeper minor groove of this B-form of DNA.

By using fluorimetric experiments, the zinc complexes show a higher affinity for GC-duplex which is not affected by the nuclearity of the complexes. Concerning single stranded RNA, poly A has comparable affinity for complexes of different nuclearity whereas poly C, poly G and poly U show an increase in affinity as the number of zinc centres in the complex increases. Circular dichroism spectra show that the binuclear complex of **PHENPOD** and the free ligand permit to identify poly A from other single stranded RNA sequences.

Lastly, antibacterial studies of the free ligands and the metal complexes in *S. aureus* and *E. coli* yield a higher inhibitory effect of the free ligands than the mono-, bi- and trinuclear zinc complexes. In addition, the ligands have higher antibacterial activity on the Gram-negative *E. coli* than on the Gram-positive bacteria *S. aureus*. It can be associated to the more negative charged membrane of *E. coli*, which can thus bind stronger to the highly positively charged ligands.

Thus, this work provides important insights into the interaction of free polyaza ligands and their corresponding zinc complexes with double and single stranded DNA/RNA as well as on the antimicrobial effect on two bacteria. The provided results will assist to constructing new systems to tackle contemporary issues such as antimicrobial resistance or DNA/RNA sensing using polynuclear metal complexes.

Experimental

Materials and apparatus

The UV-vis spectra and fluorescence spectra were recorded with a Varian Cary 100 Bio spectrometer and an Eclipse fluori-

meter, respectively. The CD spectra were registered with a JASCO J815 spectropolarimeter at 25.0 °C. Appropriate quartz cuvettes (path length: 1 cm) were used in all cases. Polynucleotides poly d(AT)₂, poly A–poly U, poly dA–poly dT, poly d(AT)₂, poly dG–poly dC, calf thymus ctDNA, poly A, poly C, poly G and poly U were purchased from Merck, and dissolved in sodium cacodylate buffer, I = 0.05 M, pH = 7.0. The ctDNA was additionally sonicated and filtered through a 0.45 mm filter to obtain mostly short (*ca.* 100 base pairs) rod-like β-helical DNA fragments.[34] The polynucleotide concentration was determined spectroscopically as the concentration of phosphates (corresponds to c(nucleotide)).[35]

Fluorimetric titrations and calculation of binding constants

Fluorimetric titrations were performed by adding aliquots of polynucleotide stock solutions to a solution of **PHENPOD** and Zn₂**PHENPOD** ($c = 1 \times 10^{-5}$ M), using $\lambda_{exc} = 320$ nm and monitoring the change in emission ($\lambda_{em} = 374$ nm) in sodium cacodylate buffer I = 0.05 M, pH = 7.0. The titrations were analysed according to the independent-site model by non-linear fitting to eqn (1),[36] in which F_0 is the initial fluorescence intensity in the absence of DNA, Q is the fluorescence enhancement upon saturation, $A = [K_a c(\text{complex})]^{-1}$ and $x = nc(\text{DNA})c(\text{complex})^{-1}$, n is the putative number of binding sites on a given polynucleotide matrix. The parameters Q and A were found by a Levenberg–Marquardt fitting routine using the Origin 8.5 software, whereas n was varied to obtain the best fit.

$$\frac{F}{F_0} = 1 + \frac{Q-1}{2}\left(A + x + 1 - \sqrt{(A+x+1)^2 - 4x}\right) \quad (1)$$

Circular dichroism spectroscopy

Circular dichroism (CD) spectra were recorded with a scanning speed of 200 nm min⁻¹ (an average of three accumulations). The buffer background was subtracted from each spectrum. CD experiments were performed by adding portions of the compound stock solution into a solution of polynucleotide ($c(\text{DNA}) = 1 \times 10^{-5}$ M).

UV thermal denaturation experiments

Thermal melting curves for ds-DNA, ds-RNA, with and without the complexes were determined by following the absorption change at 260 nm as a function of temperature.[37] The initial absorbance of the ligands was subtracted from every curve, and the absorbance scale was normalized. T_m values are the midpoints of the transition curves determined from the maximum of the first derivative and checked graphically by the tangent method. The ΔT_m values were calculated by subtracting the T_m of the free nucleic acid from the T_m of the complex. Every ΔT_m value reported is the average of at least two measurements. The error in ΔT_m is ±0.5 °C.

Crystallographic structure determination

Crystals of [Zn₂**PYPOD**Cl]Na₀.₅3.5(ClO₄)H₂O suitable for single crystal X-ray diffraction were measured in an Enraf-Nonius

KAPPA CCD single-crystal diffractometer using MoK$_\alpha$ radiation (λ = 0.71073 Å). The structure was solved by direct methods using SIR2004.[38] The structure obtained was refined using least-squares refinement, isotropically at the beginning and then anisotropically by means of the program SHELXL-2018.[39] An empirical absorption correction was applied using PLATON's MULABS routine.[40] Hydrogen atoms were placed using a riding model with the appropriate restraints, except for the solitary water molecule for which the hydrogen atoms were fixed taking into account the surrounding hydrogen bond network. Crystal data, data collection parameters, and results of the analyses are listed in Tables S1 and S2.† The crystal data has been deposited in the CSD database with deposition number 2191006.†

Assessment of the antibacterial activity

S. aureus CECT 239 and *E. coli* CECT 405 were maintained in Mueller-Hinton (MH) broth or agar at 37 °C. The antibacterial activity was evaluated by the broth microdilution plate method according to CLSI criteria against ESKAPE pathogens. Briefly, serial dilutions of the compounds were prepared in MHB (1:2 dilutions) in 96-well plates. Ciprofloxacin was used as the positive control. An initial inoculum of every strain was prepared at 0.5 McFarland in water and immediately diluted in MHB (1:20). Then, plates were inoculated with 5 µL of the bacterial dilution leading to a concentration of 5×10^5 CFU mL^{-1} and incubated at 37 °C for 18–20 h. The uninoculated broth was used as the sterility control and the inoculated broth without drugs was used as the growth control.

Author contributions

J. G.-G. performed the nucleic acids experiments. S. L.-M., C. G., C. G.-R. and M. A. D.-A. conducted the bacterial assays. S. B. diffracted and analysed the X-ray structure. I. P., E. G.-E., M. R. S. and J. G.-G. supervised and obtained the funding. J. G.-G. wrote the original manuscript. I. P., E. G.-E., M. R. S. and J. G.-G. reviewed and edited the final draft.

Conflicts of interest

There are no conflicts to declare.

Acknowledgements

References

1 K. D. Mjos and C. Orvig, *Chem. Rev.*, 2014, **114**, 4540–4563.
2 S. Medici, M. Peana, V. M. Nurchi, J. I. Lachowicz, G. Crisponi and M. A. Zoroddu, *Coord. Chem. Rev.*, 2015, **284**, 329–350.
3 T. W. Hambley, *Dalton Trans.*, 2007, **43**, 4929–4937.
4 E. J. Anthony, E. M. Bolitho, H. E. Bridgewater, O. W. L. Carter, J. M. Donnelly, C. Imberti, E. C. Lant, F. Lermyte, R. J. Needham, M. Palau, P. J. Sadler, H. Shi, F.-X. Wang, W.-Y. Zhang and Z. Zhang, *Chem. Sci.*, 2020, **11**, 12888–12917.
5 D. M. Griffith, H. Li, M. V. Werrett, P. C. Andrews and H. Sun, *Chem. Soc. Rev.*, 2021, **50**, 12037–12069.
6 R. Wang, H. Li, T. K.-Y. Ip and H. Sun, *Adv. Inorg. Chem.*, 2020, **75**, 183–205.
7 W. Sim, R. T. Barnard, M. A. T. Blaskovich and Z. M. Ziora, *Antibiotics*, 2018, **7**, 93.
8 J.-Y. Maillard and P. Hartemann, *Crit. Rev. Microbiol.*, 2013, **39**, 373–383.
9 C. N. Morrison, K. E. Prosser, R. W. Stokes, A. Cordes, N. Metzler-Nolte and S. M. Cohen, *Chem. Sci.*, 2020, **11**, 1216–1225.
10 T. GIanferrara, I. Brastos and E. Alessio, *Dalton Trans.*, 2009, 7588–7598.
11 A. Frei, J. Zuegg, A. G. Elliott, M. Baker, S. Braese, C. Brown, F. Chen, C. G. Dowson, G. Dujardin, N. Jung, A. P. King, A. M. Mansour, M. Massi, J. Moat, H. A. Mohamed, A. K. Renfrew, P. J. Rutledge, P. J. Sadler, M. H. Todd, C. E. Willans, J. J. Wilson, M. A. Cooper and M. A. T. Blaskovich, *Chem. Sci.*, 2020, **11**, 2627–2639.
12 A. Frei, *Antibiotics*, 2020, **9**, 90.
13 J. Wheate and J. G. Collins, *Coord. Chem. Rev.*, 2003, **241**, 133–145.
14 R. Lengacher, A. Marlin, D. Smilowics and E. Boros, *Chem. Soc. Rev.*, 2022, **51**, 7715–7731.
15 L. Guijarro, M. Inclan, J. Pitarch-Jarque, A. Domenech-Carbo, J. U. Chicote, S. Trefler, E. Garcia-Espana, A. Garcia-Espana and B. Verdejo, *Inorg. Chem.*, 2017, **56**, 13748–13758.
16 A. Martinez-Camarena, M. Savastano, S. Blasco, E. Delgado-Pinar, C. Giorgi, A. Bianchi, E. Garcia-España and C. Bazzicalupi, *Inorg. Chem.*, 2022, **61**, 368–383.
17 L. Acosta-Rueda, E. Delgado-Pinar, J. Pitarch-Jarque, A. Rodriguez, S. Blasco, J. Gonzalez, M. G. Basallote and E. Garcia-Espana, *Dalton Trans.*, 2015, **44**, 8255–8266.
18 M. Inclán, M. T. Albelda, J. C. Frías, S. Blasco, B. Verdejo, C. Serena, C. Salat-Canela, M. L. Díaz, A. García-España

and E. García-España, *J. Am. Chem. Soc.*, 2012, **134**, 9644–9656.

19 G. Ambrosi, M. Formica, V. Fusi, L. Giorgi, A. Guerri, M. Micheloni, P. Paoli, R. Pontellini and P. Rossi, *Inorg. Chem.*, 2007, **46**, 4737–4748.

20 G. Ambrosi, M. Formica, V. Fusi, L. Giorgi, E. Macedi, M. Micheloni, P. Paoli and P. Rossi, *Inorg. Chem.*, 2009, **48**, 10424–10434.

21 G. Ambrosi, C. Battelli, M. Formica, V. Fusi, L. Giorgi, E. Macedi, M. Micheloni, R. Pontellini and L. Prodi, *New J. Chem.*, 2009, **33**, 171–180.

22 L. Guijarro, A. Martinez-Camarena, J. U. Chicote, A. Garcia-Espana, E. Garcia-Espana, M. Inclan, B. Verdejo and J. Gonzalez-Garcia, *Molecules*, 2021, **26**, 3957.

23 J. González-García, Á. Martínez-Camarena, B. Verdejo, M. P. Clares, C. Soriano, E. Garcia-España, H. R. Jimenez, A. Domenech-Carbo, R. Tejero, E. Calvo, L. Briansó-Llort, C. Serena, S. Trefler and A. Garcia-España, *J. Inorg. Biochem.*, 2016, **163**, 230–239.

24 J. González, J. M. Llinares, R. Belda, J. Pitarch, C. Soriano, R. Tejero, B. Verdejo and E. García-España, *Org. Biomol. Chem.*, 2010, **8**, 2367–2376.

25 C. E. Castillo, M. A. Máñez, J. González, J. M. Llinares, H. R. Jimenez, M. G. Basallote and E. García-España, *Chem. Commun.*, 2010, **46**, 6081–6083.

26 C. E. Castillo, J. González-García, J. M. Llinares, M. A. Máñez, H. R. Jimenez, E. García-España and M. G. Basallote, *Dalton Trans.*, 2013, **42**, 6131–6141.

27 J. González-García, L. Uzelac, M. Kralj, I. Piantanida and E. García-España, *Org. Biomol. Chem.*, 2013, **11**, 2154–2161.

28 M. R. Stojkovic, J. Gonzalez-Garcia, F. Supljika, C. Galiana-Rosello, L. Guijarro, S. A. Gazze, L. W. Francis, I. Piantanida and E. Garcia-España, *Int. J. Biol. Macromol.*, 2018, **109**, 143–151.

29 S. Blasco, B. Verdejo, M. P. Clares, C. E. Castillo, A. G. Algarra, J. Latorre, M. A. Máñez, M. G. Basallote, C. Soriano and E. García-España, *Inorg. Chem.*, 2010, **49**, 7016–7027.

30 A. Bencini, A. Bianchi, E. Garcia-Espana, M. Giusti, S. Mangani, M. Micheloni, P. Orioli and P. Paoletti, *Inorg. Chem.*, 1987, **26**, 3902–3907.

31 A. Bencini, A. Bianchi, P. Dapporto, E. García-España, M. Micheloni, J. A. Ramirez, P. Paoletti and P. Paoli, *Inorg. Chem.*, 1992, **31**, 1902–1908.

32 J. Aragó, A. Bencini, A. Bianchi, A. Domenech and E. García-España, *J. Chem. Soc., Dalton Trans.*, 1992, 319–324.

33 S. Neidle, *Oxford handbook of nucleic acid structure*, Oxford University Press, Oxford, UK, 1999.

34 I. Orehovec, D. Glavac, I. Dokli, M. Gredicak and I. Piantanida, *Croat. Chem. Acta*, 2017, **90**, 603–611.

35 J. D. McGhee and P. H. Von Hippel, *J. Mol. Biol.*, 1974, **86**, 469–489.

36 F. H. Stootman, D. M. Fisher, A. Rodger and J. R. Aldrich-Wright, *Analyst*, 2006, **131**, 1145–1151.

37 J. L. Mergny and L. Lacroix, *Oligonucleotides*, 2003, **13**, 515–537.

38 M. C. Burla, R. Caliandro, M. Camalli, B. Carrozzini, G. L. Cascarano, L. De Caro, C. Giacovazzo, G. Polidori and R. Spagna, *J. Appl. Crystallogr.*, 2005, **38**, 381–388.

39 G. M. Sheldrick, *Acta Crystallogr., Sect. C: Struct. Chem.*, 2015, **71**, 3–8.

40 R. H. Blessing, *Acta Crystallogr., Sect. A: Found. Crystallogr.*, 1995, **51**, 33–38.